How does the northern-winter wave driving of the Brewer-Dobson circulation increase in an enhanced-CO$_2$ climate simulation?

A. J. Haklander,[1,2] P. C. Siegmund,[2] M. Sigmond,[3] and H. M. Kelder[1,2]

[1]   Recent climate studies show that the northern-winter wave driving of the Brewer-Dobson circulation is enhanced if greenhouse gas concentrations increase. An explanation for this enhancement does not yet exist. In this study, the enhanced wave driving, as simulated in a doubled-CO$_2$ experiment with the MA-ECHAM4 climate model, is analyzed in detail. The extratropical poleward eddy heat flux increases (decreases) in the stratosphere (troposphere) mainly due to the stationary (transient) heat-flux component. The heat flux at 100 hPa is a measure of the stratospheric wave driving, and is found to increase by 12% in the doubled-CO$_2$ climate. This increase is dominated by the stationary-wave 1 heat flux, which is also enhanced in the midlatitude troposphere. The heat flux increase at 100 hPa is almost entirely due to an increase in the longitudinal temperature variability. The latter increase is mainly due to the well-understood sharpening of the lower-stratospheric meridional temperature gradient. **Citation:** Haklander, A. J., P. C. Siegmund, M. Sigmond, and H. M. Kelder (2008), How does the northern-winter wave driving of the Brewer-Dobson circulation increase in an enhanced-CO$_2$ climate simulation?, *Geophys. Res. Lett.*, *35*, L07702, doi:10.1029/2007GL033054.

1.   Introduction

[2]   Global-mean CO$_2$ concentrations have risen by about 10% in the 1979–2002 period, but a structural trend in the planetary-wave driving of the Brewer-Dobson circulation (BDC) is not yet observed during northern winter, likely due to a low signal-to-noise ratio over this relatively short period [e.g., *Haklander et al.*, 2007]. However, *Butchart et al.* [2006] recently found that a more substantial increase of greenhouse gas (GHG) concentrations yields an overall strengthening of the BDC and the associated upward propagation of planetary-wave activity, with the strongest trend during northern winter. They found this result by comparing the response of the BDC to increasing GHG concentrations in an ensemble of general circulation models (GCM), with some models including interactive chemistry. The causes and nature of the strengthening are not yet clear. *Shindell et al.* [1999] suggested that increased GHG concentrations enhance the subtropical jet, so that more tropospheric planetary-wave activity at midlatitudes propagates into the stratosphere, thereby strengthening the BDC. The

physical explanation of this was, that near 200 hPa, the meridional temperature gradient increases due to lower-stratospheric cooling on the poleward side and upper-tropospheric warming on the equatorward side of the subtropical jet. The associated enhancement of the subtropical jet would then cause a decrease in the equatorward refraction of tropospheric wave activity at midlatitudes. *Eichelberger and Hartmann* [2005] studied the qualitative effect of increasing GHG concentrations on the BDC by imposing a tropical tropospheric heat source in their GCM. This dry hydrostatic GCM had a flat lower boundary, and therefore did not simulate stationary waves at all. It was found that the BDC strengthens in response to the imposed tropospheric tropical heating, with an increase in upward propagation of transient wave-2 and wave-5 activity in the troposphere. However, only the transient wave-2 increase extended upward into the stratosphere.

[3]   *Sigmond et al.* [2004] compared the BDC in a control climate and a doubled-CO$_2$ climate simulation. The BDC was found to be significantly stronger in the doubled-CO$_2$ run. Although the vertical component of the Eliassen-Palm (EP) flux increased in the midlatitude lower stratosphere, a decrease was found in the midlatitude troposphere. *Sigmond et al.* [2004] concluded that this might be caused either by a higher transparancy of the NH midlatitude tropopause for tropospheric wave activity, or by more generation of wave activity near the tropopause. Also, a modification of the gravity-wave spectrum could alter the wave driving of the BDC during northern winter. In the present study, the processes via which the resolved wave driving of the BDC could increase in an enhanced-CO$_2$ climate are examined in greater detail, using the same climate simulations as used by *Sigmond et al.* [2004].

2.   Climate Simulations and Methods

[4]   This study compares two climate simulations which have been performed by *Sigmond et al.* [2004], using the middle-atmosphere (MA) version of the ECHAM4 model [*Manzini et al.*, 1997; *Roeckner et al.*, 1996]. The model has a T42 horizontal spectral resolution (about 2.8° × 2.8°), with 39 vertical levels between the surface and 0.01 hPa (about 80 km). Momentum deposition by sub-grid scale waves is parameterized for both orographic gravity waves [*McFarlane*, 1987] and for a transient gravity-wave spectrum [*Hines*, 1997a, 1997b]. One simulation is a 30-yr control run, in which CO$_2$ concentrations were fixed at 353 ppmv. In the perturbation run, CO$_2$ concentrations were doubled. The prescribed sea-surface temperatures were obtained from a control run and a doubled-CO$_2$ run with the ECHAM4 model coupled to a slab layer ocean model.

---
[1]Department of Applied Physics, Eindhoven University of Technology, Eindhoven, Netherlands.
[2]Climate and Seismology Department, Royal Netherlands Meteorological Institute, De Bilt, Netherlands.
[3]Department of Physics, University of Toronto, Toronto, Ontario, Canada.

[5] We use the zonal-mean poleward eddy heat flux $[v*T*]$ as a measure of the net zonal-mean upward flux of planetary-wave activity, since $[v*T*]$ is proportional to the vertical component of the EP flux for quasigeostrophic waves. We define H_{100} as the average of $[v*T*]$ at 100 hPa over January–February and 40°–80°N. This (or a similar) diagnostic has been used in several studies [e.g., *Austin et al.*, 2003; *Haklander et al.*, 2007]. By partitioning the response of H_{100} to the CO$_2$ doubling into its stationary and transient components for different zonal wavenumbers, we examine the causes and nature of the increase in the northern mid-winter wave driving in greater detail. Here, the zonal wavenumber-k component of $[v*T*]$ is defined as the zonal-mean product of the wave-k components of v and T.

[6] Additionally, the poleward eddy heat flux is decomposed by noting that it equals the zonal covariance between v and T, i.e.,

$$[v*T*] = r_{v,T}\sigma_v\sigma_T, \qquad (1)$$

where $r_{v,T}$ is the zonal correlation coefficient of v and T, and σ_v and σ_T are the zonal standard deviations of v and T. Both σ_v and σ_T are indicators of wave amplitude, while $r_{v,T}$ is a measure of how effectively waves transport the sensible heat poleward. For monochromatic waves, $r_{v,T}$ is directly proportional to the cosine of the zonal phase difference between the v and T fields. CO$_2$ doubling could modify both the amplitude of the waves and the efficacy of the poleward eddy heat transport.

[7] By definition, H_{100} is obtained by evaluating the l.h.s. of Equation 1 at 100 hPa and averaging over January–February and 40°–80°N. If the three r.h.s. terms are averaged over January–February and 40°–80°N separately, the product of those averages might be different from the average of the single-variable product, due to intraseasonal and meridional cross-correlations between $r_{v,T}$, σ_v, and σ_T. Averaging the three factors on the r.h.s. of Equation 1 over January–February and 40°–80°N at 100 hPa, and multiplying them, yields an approximation of H_{100} which can be compared to H_{100} itself. For both runs, the 30-year timeseries of this approximation of H_{100} follows that of H_{100} itself very closely: correlation coefficients are 0.96 and 0.89 for the control and doubled-CO$_2$ runs, respectively. Henceforth, to keep notation simple, $r_{v,T}$, σ_v, and σ_T will denote the corresponding averages over January–February and 40°–80°N at 100 hPa. We examine if the difference in H_{100} between the control and doubled-CO$_2$ runs can be understood in terms of the differences in $r_{v,T}$, σ_v, and σ_T. These decompositions of the poleward eddy heat flux have been discussed in more detail by *Haklander et al.* [2007, section 2.3]. In the present paper, the uncertainties provided along with the estimates represent the 95% confidence intervals. Differences between the control run and the doubled-CO$_2$ run are considered statistically significant if the confidence level exceeds 95%.

3. Results

[8] We first examine the effect of CO$_2$ doubling on H_{100} by comparing the 30-year averages of the control and doubled-CO$_2$ runs. The result is shown in Table 1, along with the same comparison for several wave components of H_{100}. The total H_{100} control-run average of 15.0 ± 0.9 K m/s agrees remarkably well with the observed 1979–2002 average of 15.1 ± 1.1 K m/s in the ERA-40 dataset [*Haklander et al.*, 2007]. In our model, doubling the CO$_2$ concentrations yields a significant and substantial increase in H_{100} of 1.8 ± 1.2 K m/s, or $12\% \pm 8\%$ of the control average.

[9] In both the control and the perturbation run, stationary waves dominate the influx of planetary wave activity into the lower stratosphere. Doubling the CO$_2$ concentration in the model yields a significant stationary-wave flux increase of $23\% \pm 16\%$, determining almost entirely the total H_{100} increase. The stationary-wave flux increase occurs mainly in its stationary wave-1 component. Of the longest five stationary zonal wave components, only wavenumber 1 exhibits a noticeable change. This suggests that the total wave response to the CO$_2$ doubling can mainly be attributed to stationary wave 1. Considering the transient waves, we find a significant and substantial reduction in the transient wave-1 flux. However, this reduction is neutralized by small increases in the transient wave 2–5 components. Although the change in the transient wave 2–4 components is not significant, the statistical significance of the increase in the transient wave-5 flux is extremely high. Figures 1 and 2 show a large vertical coherence near 100 hPa. At the adjacent model levels (70 and 150 hPa), the increases in 'H_{70}' and 'H_{150}' are 1.3 ± 1.5 K m/s ($8\% \pm 9\%$), and 0.6 ± 1.2 K m/s ($4\% \pm 7\%$), respectively. The significant changes in the stationary wave-1, and transient wave-1 and wave-5 fluxes are also found at 70 and 150 hPa, with the dominant change being an increase in the stationary wave-1 flux.

[10] So far, we have only discussed 40°–80 °N averages at 100 hPa, and not yet considered the pattern of the difference in $[v*T*]$ in the meridional plane. It was men-

Table 1. The 30-Year Averages for Run C and Run A and Differences Between the A- and C-Runs for H_{100} and Its Total, Stationary and Transient $k = 1–5$ Components[a]

Component	C-Run Mean, K m/s	A-Run Mean, K m/s	Differences, K m/s	Relative Differences, %
Total	**15.0 ± 0.9**	**16.8 ± 0.8**	**+1.8 ± 1.2**	**+12% ± 8%**
Stationary	**8.6 ± 1.0**	**10.6 ± 0.9**	**+2.0 ± 1.3**	**+23% ± 16%**
Transient	6.4 ± 0.6	6.2 ± 0.5	−0.1 ± 0.8	−2% ± 12%
Total 1	8.6 ± 1.0	9.2 ± 0.7	+0.6 ± 1.2	+7% ± 14%
Total 2	3.2 ± 0.7	3.4 ± 0.5	+0.3 ± 0.8	+8% ± 26%
Total 3	1.7 ± 0.4	2.1 ± 0.3	+0.4 ± 0.5	+24% ± 27%
Total 4	0.5 ± 0.2	0.5 ± 0.2	+0.1 ± 0.3	+12% ± 56%
Total 5	**0.5 ± 0.1**	**0.9 ± 0.1**	**+0.4 ± 0.2**	**+86% ± 40%**
Stationary 1	**6.5 ± 1.0**	**8.2 ± 0.7**	**+1.7 ± 1.3**	**+27% ± 20%**
Stationary 2	1.7 ± 0.6	1.8 ± 0.5	+0.1 ± 0.8	+5% ± 46%
Stationary 3	0.5 ± 0.3	0.6 ± 0.2	+0.1 ± 0.4	+26% ± 80%
Stationary 4	−0.2 ± 0.1	−0.2 ± 0.1	+0.0 ± 0.1	+1% ± 60%
Stationary 5	0.1 ± 0.1	0.2 ± 0.0	+0.1 ± 0.1	+49% ± 59%
Transient 1	**2.2 ± 0.4**	**1.1 ± 0.3**	**−1.1 ± 0.5**	**−51% ± 25%**
Transient 2	1.5 ± 0.4	1.6 ± 0.3	+0.2 ± 0.5	+12% ± 35%
Transient 3	1.2 ± 0.3	1.5 ± 0.2	+0.3 ± 0.3	+23% ± 28%
Transient 4	0.7 ± 0.1	0.8 ± 0.2	+0.1 ± 0.2	+8% ± 30%
Transient 5	**0.4 ± 0.1**	**0.7 ± 0.1**	**+0.4 ± 0.1**	**+99% ± 45%**

[a]Also provided are the 95% confidence intervals. Components for which the differences are >95% significant are given in bold.
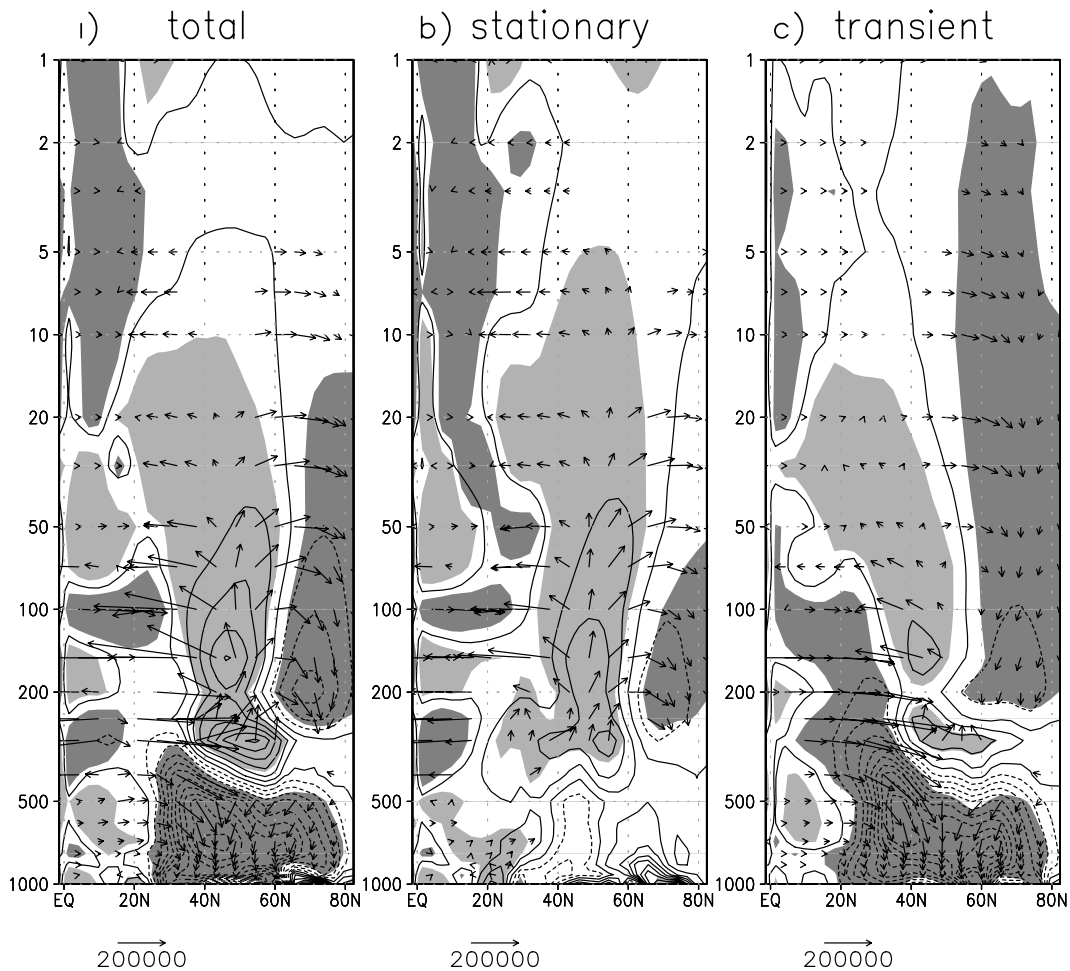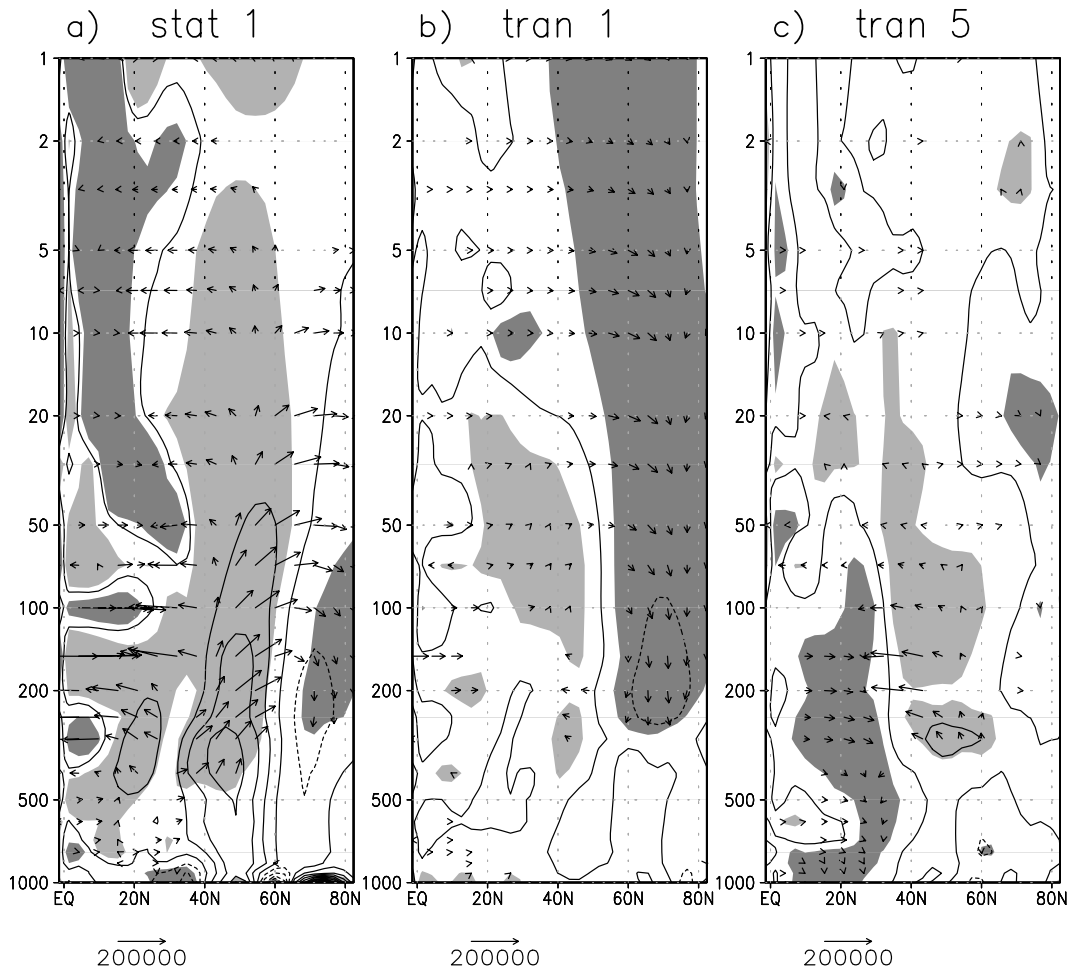
Figure 1. Meridional cross sections of the mean difference in EP flux vectors (doubled-CO$_2$ – control run) for the (a) total, (b) stationary, and (c) transient waves. Difference vectors are drawn only if the difference in at least one of the two EP flux components is statistically significant at the 95% confidence level. The vectors have been scaled by multiplying with e$^{z/H}$ (where the scale height H = 7 km) and the meridional components have been divided by 70 to account for the aspect ratio of the plots. Contours indicate the difference in the (unscaled) vertical EP flux. Negative contour lines are dashed, and the contour interval is 2×10^4 m^3 s^{-2}. Significantly (95%) positive and negative values are shaded light and dark, respectively.

tioned in the previous section, that for quasigeostrophic waves $[v*T*]$ is proportional to the vertical component of the EP flux. The meridional pattern of the EP-flux vector differences can elucidate the effect of CO$_2$ doubling on the propagation of planetary-wave activity. Figure 1 shows these difference patterns for the total, stationary and transient components of the EP flux. At midlatitudes between 400 and 10 hPa, the total upward EP flux increases significantly. A significant decrease is found in the troposphere north of about 25°N. In the stratosphere the total wave response (Figure 1a) is similar to the stationary-wave response (Figure 1b), whereas in the troposphere it is more similar to the transient-wave response (Figure 1c). In the subtropical troposphere, the doubled-CO$_2$ run exhibits significantly less equatorward propagation of (transient) wave activity, indicated by the poleward orientation of the EP flux difference vectors in Figures 1a and 1c. Starting in the subtropical troposphere and following the difference vectors according to ray-tracing theory, we see that the subtropical reduction of equatorward wave propagation is likely asso-

ciated with less transient upward wave propagation in the midlatitude (lower) troposphere to begin with. The latter is expected to be due to a decrease in baroclinicity, since the tropospheric pole-to-equator temperature gradient is reduced in the perturbation run [*Sigmond et al.*, 2004] (Figure 2a).

[11] Since a significant difference between the control and perturbation runs was found for the stationary wave-1 and transient wave-1 and wave-5 components of H_{100}, we also show the meridional cross sections of the EP flux difference for those three wave components in Figure 2. For stationary wave-1 (Figure 2a), a marked increase in the upward EP flux is observed particularly at midlatitudes, although the increase is not significant in the lower troposphere. Nevertheless, the contour pattern in Figure 2a indicates that the increase in stationary wave-1 activity flux at 100 hPa is associated with an increase in upward stationary wave-1 flux in the entire troposphere. Table 1 suggests that the total wave response to the CO$_2$ doubling can mainly be attributed to stationary wave 1. This is

Figure 2. Meridional cross sections of the mean difference in EP flux vectors (doubled-CO$_2$ – control run) for the (a) stationary-1, (b) transient-1, and (c) transient-5 wave components. Scaling, contours, and shading as in Figure 1.

confirmed by the strong similarity in the lower stratosphere between the total difference pattern in Figure 1a and the stationary wave-1 difference pattern in Figure 2a. Figure 2b shows that the substantial decrease in the transient wave-1 component of H_{100} is due to a flux decrease north of about 52°N. The EP-flux difference for the transient wave-5 component at 100 hPa (Figure 2c) exhibits a significant increase at midlatitudes.

[12] We next examine the effect of CO$_2$ doubling on the amplitude of the waves, and their correlation, as described in the previous section. Table 2 shows the 30-year averages and differences for H_{100}, its approximate value $r_{v,T}\,\sigma_v\,\sigma_T$, and $r_{v,T}$, σ_v, and σ_T. The increase in $r_{v,T}\,\sigma_v\,\sigma_T$ in the doubled-CO$_2$ climate is statistically significant and quantitatively

comparable to the increase in H_{100}. The changes in $r_{v,T}$ are very small and not significant. However, the zonal standard deviations of both v and T do show a significant increase. Whereas σ_v exhibits only a marginal increase, the increase in σ_T is found to be the dominant cause of the increased wave driving. Not only is the change in σ_T significant, the relative change is substantial (+12%± 5%) and comparable to the change in H_{100} (+12% ± 8%). A significant increase in σ_T is also found at 70 and 150 hPa, and the percent increase in σ_T is comparable with the percent increase in the total heat flux at both levels (not shown). In Figure 3, the January–February mean total eddy temperature field at 100 hPa is shown for the control and the perturbation runs. The stationary wave-1 signature is well visible for both experi-

Table 2. The 30-Year Averages for the Control and Doubled-CO$_2$ Runs and Differences Between the Two Runs in H_{100} and $r_{v,T}\,\sigma_v\,\sigma_T$ and the Separate Factors $r_{v,T}$, σ_v, and σ_T[a]

Component	Control	2 × CO$_2$	Differences	Relative Differences, %
H_{100}, K m/s	**15.0 ± 0.9**	**16.8 ± 0.8**	**+1.8 ± 1.2**	**+12% ± 8%**
$r_{v,T}\,\sigma_v\,\sigma_T$, K m/s	**14.1 ± 0.9**	**16.4 ± 0.8**	**+2.3 ± 1.2**	**+16% ± 8%**
$r_{v,T}$	0.213 ± 0.007	0.216 ± 0.013	+0.002 ± 0.015	+1% ± 7%
σ_v, m/s	**10.1 ± 0.2**	**10.5 ± 0.3**	**+0.4 ± 0.4**	**+4% ± 3%**
σ_T, K	**6.5 ± 0.2**	**7.3 ± 0.2**	**+0.8 ± 0.3**	**+12% ± 5%**

[a]Also provided are the 95% confidence intervals. Components for which the differences are 95% significant are given in bold.
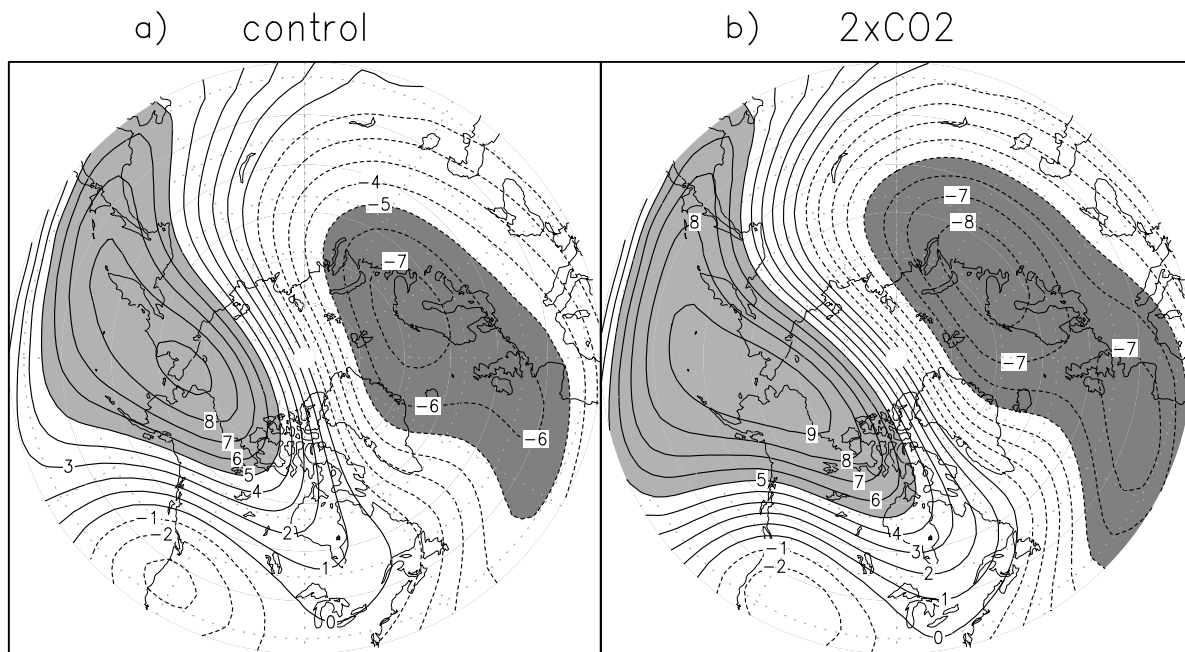
Figure 3. January–February mean eddy temperature field T^* at 100 hPa, for (a) the control run, and (b) the doubled-CO_2 run. Light and dark shading indicate eddy temperatures above +5K and below −5K, respectively. The contour interval is 1K.

ments, and Figure 3 clearly demonstrates the increase in longitudinal temperature variability in the doubled-CO_2 run. The increase in σ_T may be due to an increase in the meridional temperature gradient between $40°–80°N$ at 100 hPa, as meridional air displacements will produce larger zonal temperature asymmetries if the zonal-mean meridional temperature gradient increases. Indeed, the 30-year average January–February temperature difference between $40°N$ and $80°N$ at 100 hPa increases by about 10% in the perturbation run (not shown). Below 400 hPa, the temperature difference between $40°N$ and $80°N$ decreases in the doubled-CO_2 run, with the largest reduction in the lower troposphere. This result agrees with the significant reduction in midlatitude upward EP flux at those levels that was discussed above.

4. Conclusion

[13] In this paper, the effect of CO_2 doubling on the northern-winter upward wave activity flux at midlatitudes has been analyzed, using the MA-ECHAM4 climate model. The upward wave flux is quantified by H_{100}, defined as the average of $[v^*T^*]$ at 100 hPa over January–February and $40°–80°N$. Doubling the CO_2 concentration leads to a substantial and significant increase in H_{100} of 1.8 ± 1.2 K m/s, or 12% ± 8%. This is, at least qualitatively, in agreement with the studies by, e.g., *Butchart and Scaife* [2001], *Rind et al.* [1998, 2002], and *Butchart et al.* [2006]. Table 1 and Figures 1a and 2a indicate that stationary-wave 1 likely accounts for almost all of the total increase in H_{100}. This suggests that at least part of the increase is due to more stationary wave-1 generation at midlatitudes in the (lower) troposphere. The results indicate that doubling the CO_2 yields significant changes in transient wave-1 and transient wave-5 as well. The latter change is in agreement with the

result of *Eichelberger and Hartmann* [2005], but their model setup (no topography) was quite different from that in the present study. Transient wave-5 may not seem very relevant due to its small contribution, but its increase amounts to 19 ± 15% of the total H_{100} increase.

[14] Using an alternative decomposition of the poleward eddy heat flux, we found that the increased wave driving can be attributed mainly to a larger longitudinal temperature variability, that is mainly due to the increased meridional temperature gradient at 100 hPa in the doubled-CO_2 climate simulation. With only one climate model at our disposal, we were not able to test the robustness of our results. However, both the increase in the northern-winter wave driving of the BDC and the increase in the 100-hPa meridional temperature gradient are robust features in enhanced-CO_2 climate simulations. We would welcome studies in which our analysis method is applied to data from other enhanced-CO_2 simulations.

References

Austin, J., et al. (2003), Uncertainties and assessments of chemistry-climate models of the stratosphere, *Atmos. Chem. Phys.*, 3, 1–27.

Butchart, N., and A. A. Scaife (2001), Removal of CFCs through increased mass exchange between the stratosphere and troposphere in a changing climate, *Nature*, 410, 799–801.

Butchart, N., et al. (2006), Simulations of antropogenic change in the strength of the Brewer-Dobson circulation, *Clim. Dyn.*, 27, 727–741, doi:10.1007/s00382-006-0162-4.

Eichelberger, S. J., and D. L. Hartmann (2005), Changes in the strength of the Brewer-Dobson circulation in a simple AGCM, *Geophys. Res. Lett.*, 32, L15807, doi:10.1029/2005GL022924.

Haklander, A. J., P. C. Siegmund, and H. M. Kelder (2007), Interannual variability of the stratospheric wave driving during northern winter, *Atmos. Chem. Phys.*, 7, 2575–2584.

Hines, C. O. (1997a), Doppler-spread parameterization of gravity-wave momentum deposition in the middle atmosphere. part 1: Basic formulation, *J. Atmos. Sol. Terr. Phys.*, *59*, 371–386.

Hines, C. O. (1997b), Doppler-spread parameterization of gravity-wave momentum deposition in the middle atmosphere. part 2: Broad and quasi monochromatic spectra, and implementation, *J. Atmos. Sol. Terr. Phys.*, *59*, 387–400.

Manzini, E., N. A. McFarlane, and C. McLandress (1997), Impact of the Doppler spread parameterization on the simulation of the middle atmosphere circulation using the MA/ECHAM4 general circulation model, *J. Geophys. Res.*, *102*(D22), 25,751–25,762.

McFarlane, N. A. (1987), The effect of orographically excited gravity-wave drag on the general circulation of the lower stratosphere and troposphere, *J. Atmos. Sci.*, *44*, 1775–1800.

Rind, D., D. Shindell, P. Lonergan, and N. K. Balachandran (1998), Climate change and the middle atmosphere. part III: The doubled CO$_2$ climate revisited, *J. Clim.*, *11*, 876–894, doi:10.1175/1520-0442.

Rind, D., P. Lonergan, N. K. Balachandran, and D. Shindell (2002), $2 \times$ CO$_2$ and solar variability influences on the troposphere through wave-mean flow interaction, *J. Meteorol. Soc. Jpn.*, *80*, 863–876.

Roeckner, E., K. Arpe, L. Bengtsson, M. Christoph, M. Claussen, L. Dümenil, M. Esch, M. Giorgetta, U. Schlese, and U. Schulzweida (1996), The atmospheric general circulation model ECHAM-4: Model description and simulation of present-day climate, *Rep. 218*, Max Planck Inst. for Meteorol., 90 pp., Hamburg, Germany.

Shindell, D. T., R. L. Miller, G. A. Schmidt, and L. Pandolfo (1999), Simulation of recent northern winter climate trends by greenhouse-gas forcing, *Nature*, *399*, 452–455, doi:10.1038/20905.

Sigmond, M., P. C. Siegmund, E. Manzini, and H. Kelder (2004), A simulation of the separate climate effects of middle atmospheric and tropospheric CO$_2$ doubling, *J. Clim.*, *17*, 2352–2367.

────────────────

A. J. Haklander and H. M. Kelder, Department of Applied Physics, Eindhoven University of Technology, P.O. Box 513, NL-5600 MB Eindhoven, Netherlands. (haklande@knmi.nl)

P. C. Siegmund, Climate and Seismology Department, Royal Netherlands Meteorological Institute, P.O. Box 201, NL-3730 AE De Bilt, Netherlands.

M. Sigmond, Department of Physics, University of Toronto, 60 St. George St., Toronto, ON, Canada M5S 1A7.